SIViP (2011) 5:61–68
DOI 10.1007/s11760-009-0142-3

ORIGINAL PAPER

A joint 2D AM–FM estimation based on higher order Teager–Kaiser energy operators

E. H. S. Diop · A. O. Boudraa · F. Salzenstein

Received: 8 October 2008 / Revised: 1 October 2009 / Accepted: 4 October 2009 / Published online: 23 October 2009

Abstract In this work, an image demodulation algorithm based on two-dimensional higher order Teager–Kaiser (TK) operators is presented. We show quantitatively and qualitatively that the introduction of higher orders in TK operator improves amplitude modulation (AM) and frequency modulation (FM) estimation results, compared to classical approaches such as the Discrete Energy Separation Algorithm (DESA) or the Analytic Signal (AS) method. Indeed, for a wide class of images, obtained demodulation errors for both the amplitude and frequency are numerically lower than the obtained ones with the DESA and AS method. The proposed method is illustrated on both synthetic and real images. Moreover, it turns out for some real images that the algorithm is very efficient in the sense that it tracks the most significant part in images and segments regions of interests, particularly, the AM counterpart. Finally, an application of our approach to the segmentation of mines' shadows in Sonar images is presented. This is very important for both civil and military applications.

Keywords Image demodulation · Teager–Kaiser energy operator · Higher order differential energy operator · Energy separation algorithm · Discrete energy separation algorithm · Amplitude modulation · Frequency modulation

E. H. S. Diop · A. O. Boudraa (✉)
IRENav, Ecole Navale, Lanvéoc-Poulmic,
29240 Brest-Armées, France
e-mail: boudra@ecole-navale.fr

E. H. S. Diop · A. O. Boudraa
E^3I^2-EA3876, ENSIETA, Ecole Navale, Lanvéoc-Poulmic,
29240 Brest-Armées, France
e-mail: diop@ecole-navale.fr

F. Salzenstein
Laboratoire Iness, CNRS/STIC-UPR, Université Louis Pasteur,
23 rue du Loess, BP 20 CR, 67037 Strasbourg Cedex 2, France
e-mail: salzenst@iness.c-strasbourg.fr

1 Introduction

Teager–Kaiser energy operator (TKEO) was introduced by Teager and Teager [1] and extended by Kaiser for analyzing oscillatory signals with time-varying amplitude and frequency in speech processing [2]. The TKEO output for any given signal $s(t)$ is given by

$$\Psi\left[s(t)\right] = \left(\frac{\mathrm{d}s(t)}{\mathrm{d}t}\right)^2 - s(t)\frac{\mathrm{d}^2 s(t)}{\mathrm{d}t^2} \tag{1}$$

Also known as Teager energy, the TKEO is a non-linear operator. In fact, it tracks the energy to generate the signal $s(t)$. This useful instantaneous energy operator was extended, later on, to the two-dimensional (2D) case by Yu et al. [3]. Demodulating a signal of any dimension consists of finding the frequency modulation (FM) and the amplitude modulation (AM) components. In order to achieve this, many algorithms have been proposed. We can quote as examples, for 1D signals, the Energy Separation Algorithm (ESA) and its discrete version, the Discrete ESA (DESA) [4], and the 2D ESA for images [5]. Both ESA or 2D ESA rely on the TKEO [4,5]. Narrowband images, modeled as 2D spatial AM–FM signals, can be demodulated by the 2D ESA [5]. Another image demodulation approach, based on the Analytic Signal (AS), was proposed by Havlicek [6]. In this work, we mainly focus on image demodulation with energy operators.

Recently, different extensions of the TKEO were proposed to improve signals demodulation's results [7–10]. The first extension of the 1D TKEO to higher order, called k-order differential energy operator (DEO), was developed by Maragos and Potamianos [7] and later generalized by

Salzenstein et al. [9]. In [8], Salzenstein et al. presented a 2D discrete version of the DEO, and showed that the demodulation results, particularly the AM components, are better than the ones obtained with 2D TKEO. We can also quote the work of Boudraa et al. [10], who proposed an extension of both the 2D TKEO and the DEO to 2D continuous case. These 2D continuous operators allow to use a large class of image gradient filters, and consequently, different discrete energy operators were derived. Based on these operators, a 2D continuous demodulation algorithm called continuous higher order energy demodulation algorithm (CHOEDA) was developed [10].

Motivated by the works of Salzenstein et al. [8] and Boudraa et al. [10], we explore in this paper, 2D higher order Teager–Kaiser (TK) energy operators, in order to get, as for the 1D case, better image demodulation results. Our objective is to introduce higher orders in TK operator for narrowband signal demodulation and to get much lower amplitude and frequency approximation errors. As we will see throughout the paper, the 2D-DEO brings relevant additional information that cannot be carried out by the classical 2D TKEO.

The article is organized as follows: Sect. 2 presents a background review of DEO and CHOEDA. The proposed discrete image demodulation algorithm is presented in Sect. 3. In Sect. 4, numerical results for both synthetic and real images are presented. For real images, we apply the demodulation algorithm for image segmentation. Mines' shadow segmentation in Sonar images is an important application of our algorithm. This is a challenging and decisive task, especially, for civil and military applications. Concluding remarks are given in Sect. 5.

2 Higher order energy operators

2.1 Higher order Teager–Kaiser operators for 1D signals

Maragos and Potamianos proposed a generalization of the TKEO for 1D signals, along with some discretization schemes in [7]. For any signal $s(t)$, the k-order DEO applied to $s(t)$ gives

$$\Psi_k\left[s(t)\right] = \frac{\mathrm{d}s(t)}{\mathrm{d}t}\frac{\mathrm{d}^{k-1}s(t)}{\mathrm{d}t^{k-1}} - s(t)\frac{\mathrm{d}^k s(t)}{\mathrm{d}t^k} \tag{2}$$

One can easily check that the Teager energy of $s(t)$ is Ψ_2. Equation (2) represents a generalization of TKEO. Also, we got recursive relations between orders, such as

$$\Psi_k\left[s(t)\right] = \frac{\mathrm{d}}{\mathrm{d}t}\Psi_{k-1}\left[s(t)\right] - \Psi_{k-2}\left[\frac{\mathrm{d}s(t)}{\mathrm{d}t}\right] \tag{3}$$

For a cosine, $s(t) = A\cos(\omega t + \Phi)$, one has [7]:

$$\Psi_k\left[s(t)\right] = \begin{cases} 0 & \text{if } k = \pm 1, \pm 3, \ldots \\ (-1)^{1+\frac{k}{2}} A^2 \omega^k & \text{if } k = 0, \pm 2, \pm 4, \ldots \end{cases} \tag{4}$$

Either the ESA or the DESA, and the demodulation algorithm derived from DEO [7], rely on a strong assumption that the signal should be narrowband and its amplitude and frequency should not vary neither too fast, nor too greatly in value compared with the carriers [5]. We refer to carrier frequency as a constant-center frequency. Finally, one gets AM and FM components by combining the second order DEO (i.e. 2D TKEO) and the fourth order, as follows [7]:

$$\omega = \sqrt{\frac{-\Psi_4\left[s(t)\right]}{\Psi_2\left[s(t)\right]}} \tag{5}$$

$$|A| = \frac{\Psi_2\left[s(t)\right]}{\sqrt{-\Psi_4\left[s(t)\right]}} \tag{6}$$

2.2 The continuous higher order demodulation algorithm (CHODEA)

AM–FM image modeling aims to overcome the constraints of the Fourier transform, in order to get a representation capable to hold, with a given number of quasi-sinusoidal 2D AM–FM functions, the main information in images.

Image demodulation problem is the same as for the 1D case, which basically consists in finding AM and FM components. For images, the AM component captures the local texture contrast, that is the disparity in intensity between the brightest and darkest elements of the local texture pattern [11]. The FM component tells us about the local texture orientation, the image granularity, and edges in the image [11–13].

Let I be a discrete image. For simplicity, we also note by I its continuous interpolate. The image and its interpolate will be distinguished by their arguments: if we use the notation $I(k,l)$, I is the discrete image; and for $I(x_1,x_2)$, I represents the interpolated image. The 2D higher order operators will be extrapolated from

$$\begin{aligned}\phi_2\left[I(x_1,x_2)\right] = &\left[\left(\frac{\partial I}{\partial x_1}\right)^2 - I\frac{\partial^2 I}{\partial x_1^2}\right] \\ &+\left[\left(\frac{\partial I}{\partial x_2}\right)^2 - I\frac{\partial^2 I}{\partial x_2^2}\right] \\ &+2\left[\left(\frac{\partial I}{\partial x_1}\frac{\partial I}{\partial x_2}\right) - I\frac{\partial^2 I}{\partial x_1 \partial x_2}\right]\end{aligned} \tag{7}$$

The two first terms correspond to the extended 2D TKEO [3,14]. The last term constitutes the major difference. It represents the energy interaction between horizontal and vertical

directions. Equation (7) can be rewritten as

$$\begin{aligned}\phi_2[I(x_1,x_2)] &= \{\Lambda[I(x_1,x_2)]\}^2 \\ &\quad -I(x_1,x_2)\cdot\Lambda\{\Lambda[I(x_1,x_2)]\} \qquad (8)\\ &= \{\Lambda[I(x_1,x_2)]\}^2 \\ &\quad -I(x_1,x_2)\cdot\Lambda^2[I(x_1,x_2)] \qquad (9)\end{aligned}$$

where

$$\Lambda(I)=\frac{\partial I}{\partial x_1}+\frac{\partial I}{\partial x_2}$$

For the third order, one has

$$\begin{aligned}\phi_3[I(x_1,x_2)] &= \Lambda[I(x_1,x_2)]\cdot\Lambda^2[I(x_1,x_2)] \\ &\quad -I(x_1,x_2)\cdot\Lambda^3[I(x_1,x_2)]\end{aligned} \qquad (10)$$

The generalization at any order k is given by [10]:

$$\begin{aligned}\phi_k[I(x_1,x_2)] &= \Lambda[I(x_1,x_2)]\cdot\Lambda^{k-1}[I(x_1,x_2)] \\ &\quad -I(x_1,x_2)\cdot\Lambda^k[I(x_1,x_2)]\end{aligned} \qquad (11)$$

When developing Eq. (10), one gets

$$\begin{aligned}\phi_3[I(x_1,x_2)] &= (\partial_1 I(x_1,x_2)\,\partial_1^2 I(x_1,x_2) \\ &\quad -I(x_1,x_2)\,\partial_1^3 I(x_1,x_2)) \\ &\quad +(\partial_2 I(x_1,x_2)\,\partial_2^2 I(x_1,x_2) \\ &\quad -I(x_1,x_2)\,\partial_2^3 I(x_1,x_2)) \\ &\quad +(\partial_1 I(x_1,x_2)\,\partial_2^2 I(x_1,x_2) \\ &\quad +2\partial_2 I(x_1,x_2)\,\partial_{12}^2 I(x_1,x_2) \\ &\quad -3I(x_1,x_2)\,\partial_{12^2}^3 I(x_1,x_2)) \\ &\quad +(\partial_2 I(x_1,x_2)\,\partial_1^2 I(x_1,x_2) \\ &\quad +2\partial_1 I(x_1,x_2)\,\partial_{12}^2 I(x_1,x_2) \\ &\quad -3I(x_1,x_2)\,\partial_{1^2 2}^3 I(x_1,x_2))\end{aligned} \qquad (12)$$

where, for any function f of class $C^m(\mathbb{R}^2)$, $\partial_{1^p 2^q}^m(f)=\dfrac{\partial^m f}{\partial x_1^p\,\partial x_2^q}(x_1,x_2)$ with $p+q=m$.

We, then, could write (10) more simply, as

$$\phi_3[I(x_1,x_2)] = \partial_1\{\phi_2[I(x_1,x_2)]\}+\partial_2\{\phi_2[I(x_1,x_2)]\} \qquad (13)$$

One can prove by recurrence that for all $k>3$, we have

$$\begin{aligned}\phi_k[I(x_1,x_2)] &= \partial_1\{\phi_{k-1}[I(x_1,x_2)]\} \\ &\quad +\partial_2\{\phi_{k-1}[I(x_1,x_2)]\} \\ &\quad -\phi_{k-2}[\partial_1 I(x_1,x_2)+\partial_2 I(x_1,x_2)]\end{aligned} \qquad (14)$$

Let us consider an AM–FM image model given by

$$I(x_1,x_2)=a(x_1,x_2)\cos(\Omega_1 x_1+\Omega_2 x_2) \qquad (15)$$

where $a(x_1,x_2)$ denotes a slowly varying amplitude function. When applying ϕ_2 to $I(x_1,x_2)$, one has

$$\begin{aligned}\phi_2[I(x_1,x_2)] &= [a(x_1,x_2)]^2(\Omega_1+\Omega_2)^2 \\ &\quad +\cos^2(\Omega_1 x_1+\Omega_2 x_2)\cdot\phi_2[a(x_1,x_2)]\end{aligned} \qquad (16)$$

Under realistic assumptions [5], applying ϕ_2 to I yields the image energy derived as the product of the squared instantaneous amplitude and frequency magnitude [10]:

$$\phi_2[I(x_1,x_2)] \approx [a(x_1,x_2)]^2(\Omega_1+\Omega_2)^2 \qquad (17)$$

with a bounded approximation error [5,13].

Thanks to [3,10], we have

$$\begin{aligned}&\phi_3[I(x_1,x_2)]=0 \quad \text{and} \\ &\phi_4[I(x_1,x_2)] \approx -[a(x_1,x_2)]^2(\Omega_1+\Omega_2)^4\end{aligned} \qquad (18)$$

By combining Eqs. (16)–(18), we get the amplitude estimate expression $\hat{a}(x_1,x_2)$ of $a(x_1,x_2)$, as [10]

$$|\hat{a}(x_1,x_2)| = \frac{\phi_2[I(x_1,x_2)]}{\sqrt{-\phi_4[I(x_1,x_2)]}} \qquad (19)$$

One can prove that

$$\begin{aligned}&\phi_2[\partial_1 I(x_1,x_2)-\partial_2 I(x_1,x_2)] \\ &\quad \approx [a(x_1,x_2)]^2(\Omega_1-\Omega_2)^2(\Omega_1+\Omega_2)^2 \qquad (20)\\ &\phi_2[\partial_1 I(x_1,x_2)+\partial_2 I(x_1,x_2)] \\ &\quad \approx [a(x_1,x_2)]^2(\Omega_1+\Omega_2)^2(\Omega_1+\Omega_2)^2 \qquad (21)\end{aligned}$$

Putting together Eqs. (15), (20) and (21), yields

$$(\Omega_1-\Omega_2)^2 \approx \frac{\phi_2[\partial_1 I(x_1,x_2)-\partial_2 I(x_1,x_2)]}{\phi_2[I(x_1,x_2)]} \qquad (22)$$

$$(\Omega_1+\Omega_2)^2 \approx \frac{\phi_2[\partial_1 I(x_1,x_2)+\partial_2 I(x_1,x_2)]}{\phi_2[I(x_1,x_2)]} \qquad (23)$$

Let $\hat{\Omega}_1$ and $\hat{\Omega}_2$ be the estimates of Ω_1 and Ω_2. Using polar coordinates $(\|\hat{\Omega}\|,\hat{\theta})$, where $\hat{\Omega}=(\hat{\Omega}_1,\hat{\Omega}_2)$, one obtains

$$\hat{\Omega}_1=\|\hat{\Omega}\|\cos(\hat{\theta}) \quad \text{and} \quad \hat{\Omega}_2=\|\hat{\Omega}\|\sin(\hat{\theta}) \qquad (24)$$

Thanks to Eqs. (22) and (23), we have [10]

$$\|\hat{\Omega}\| = \sqrt{\frac{\phi_2[\partial_1 I(x_1,x_2)-\partial_2 I(x_1,x_2)]+\phi_2[\partial_1 I(x_1,x_2)+\partial_2 I(x_1,x_2)]}{2\phi_2[I(x_1,x_2)]}} \qquad (25)$$

$$\hat{\theta} = \frac{1}{2}\arcsin\left[\frac{\phi_2[\partial_1 I(x_1,x_2)+\partial_2 I(x_1,x_2)]-\phi_2[\partial_1 I(x_1,x_2)-\partial_2 I(x_1,x_2)]}{\phi_2[\partial_1 I(x_1,x_2)+\partial_2 I(x_1,x_2)]+\phi_2[\partial_1 I(x_1,x_2)-\partial_2 I(x_1,x_2)]}\right] \qquad (26)$$

Formulas (19), (25) and (26) constitute the algorithm CHOEDA [10].

3 Discrete higher order image demodulation algorithm

It is important to point out the discrete nature of images, especially, when using continuous algorithms such as the CHOEDA. Numerical results will highly rely on the image's interpolants. However, in this paper, we are more interested

in elaborating a discrete algorithm than trying to solve image interpolation issues.

Another drawback of the ESA and the 2D DESA [6] algorithms is that horizontal and vertical frequencies' components must range between 0 and $\frac{\pi}{2}$. Consequently, frequencies can be estimated only up to one fourth of the sampling frequency domain. This is due to the fact that actual 2D TKEO extension is just a basic extension of the 1D TKEO along the vertical and horizontal axes. It implies that other directions, such as diagonals, are not taken into account. All this lead us to go for the operator presented by Boudraa et al. [10], instead of the classical 2D TKEO. Therefore, we consider Eq. (7) as the Teager energy of the given image I.

We use the notations $I_1(k,l) = \frac{1}{2}[I(k+1,l) - I(k-1,l)]$, $I_2(k,l) = \frac{1}{2}[I(k,l+1) - I(k,l-1)]$, and $I_{12}(k,l) = \frac{1}{2}[I_2(k+1,l) - I_2(k-1,l)]$ as discretization schemes of $\frac{\partial I}{\partial x_1}$, $\frac{\partial I}{\partial x_2}$ and $\frac{\partial^2 I}{\partial x_1 \partial x_2}$, respectively. Then, Eq. (7) and its discretization schemes are written as follows:

$$\begin{aligned}\Psi_2[I(k,l)] = \{&2[I(k,l)]^2 - I(k-1,l)\,I(k+1,l)\\ &-I(k,l-1)\,I(k,l+1)\}\\ &+2[I_1(k,l)\,I_2(k,l) - I(k,l)\,I_{12}(k,l)]\end{aligned} \tag{27}$$

As mentioned earlier for the continuous case, the first term between braces is the same as the extended 2D discrete version of the TKEO, and used in the DESA. The second term represents the interaction between pixels along horizontal and vertical axes.

Let $I(k,l) = a(k,l)\cos(\Omega_1 k + \Omega_2 l)$ be a discrete image with slowly varying AM and FM components. We have

$$\Psi_2[I(k,l)] \approx [a(k,l)]^2\,(\sin(\Omega_1) + \sin(\Omega_2))^2 \tag{28}$$

$$\Psi_3[I(k,l)] = 0 \quad \text{and}$$

$$\Psi_4[I(k,l)] \approx -[a(k,l)]^2\,(\sin(\Omega_1) + \sin(\Omega_2))^4 \tag{29}$$

We also have the relations:

$$\begin{aligned}\Psi_2[I_i(k,l)] \approx\ &[a(k,l)]^2\,[\sin(\Omega_i)]^2\\ &(\sin(\Omega_1) + \sin(\Omega_2))^2\,; \quad \forall i = 1,2\end{aligned} \tag{30}$$

$$\begin{aligned}\Psi_2[I_{12}(k,l)] \approx\ &[a(k,l)]^2\,[\sin(\Omega_1)]^2\,[\sin(\Omega_2)]^2\\ &(\sin(\Omega_1) + \sin(\Omega_2))^2\end{aligned} \tag{31}$$

$$\begin{aligned}\Psi_4[I_i(k,l)] \approx\ &-[a(k,l)]^2\,[\sin(\Omega_i)]^2\\ &(\sin(\Omega_1) + \sin(\Omega_2))^4\,; \quad \forall i = 1,2\end{aligned} \tag{32}$$

$$\begin{aligned}\Psi_4[I_{12}(k,l)] \approx\ &-[a(k,l)]^2\,[\sin(\Omega_1)]^2\,[\sin(\Omega_2)]^2\\ &(\sin(\Omega_1) + \sin(\Omega_2))^4\end{aligned} \tag{33}$$

By combining Eqs. (28)–(33), we finally get the AM estimate denoted by $\hat{a}(k,l)$, and the horizontal and vertical FM estimates, respectively, denoted by $\hat{\Omega}_1$ and $\hat{\Omega}_2$. Thus

$$|\hat{a}(k,l)| = \sqrt{\frac{\Psi_2[I_1(k,l)]\cdot\Psi_2[I_2(k,l)]}{-\Psi_4[I_{12}(k,l)]}} \tag{34}$$

$$|\hat{\Omega}_1(k,l)| = \arcsin\sqrt{\frac{\Psi_2[I_{12}(k,l)]}{\Psi_2[I_2(k,l)]}} \tag{35}$$

$$|\hat{\Omega}_2(k,l)| = \arcsin\sqrt{\frac{\Psi_2[I_{12}(k,l)]}{\Psi_2[I_1(k,l)]}} \tag{36}$$

Using Eqs. (14) and (17), we have

$$\begin{aligned}\phi_4[I(x_1,x_2)] &= \partial_1\{\phi_3[I(x_1,x_2)]\} + \partial_2\{\phi_3[I(x_1,x_2)]\}\\ &\quad -\phi_2[\partial_1 I(x_1,x_2) + \partial_2 I(x_1,x_2)]\\ &= -\phi_2[\partial_1 I(x_1,x_2) + \partial_2 I(x_1,x_2)]\end{aligned}$$

Then, Eq. (34) can be rewritten as

$$|\hat{a}(k,l)| = \sqrt{\frac{\Psi_2[I_1(k,l)]\cdot\Psi_2[I_2(k,l)]}{\Psi_2\left[I^1_{12}(k,l) + I^2_{12}(k,l)\right]}} \tag{37}$$

where $I^1_{12}(k,l) = \frac{1}{2}\left[I_{12}(k+1,l) - I_{12}(k-1,l)\right]$, and $I^2_{12}(k,l) = \frac{1}{2}[I_{12}(k,l+1) - I_{12}(k,l-1)]$

Formulas (34)–(37) constitute the demodulation algorithm, which we refer from now on, to the discrete higher order demodulation algorithm (DHODA).

4 Numerical results

The DHODA is applied to synthetic and real images to show its efficiency. Results are compared to the DESA algorithm and the AS approach.

4.1 Synthetic images

The DHODA and the DESA are applied to a 2D AM–FM signal (cf. Fig. 1), defined by

$$\begin{aligned}I(k,l) = 0.5&\left[1 + 0.5\cos\left(k\frac{\pi}{30} + l\frac{\pi}{50}\right)\right]\cos\left[k\frac{\pi}{3} + l\frac{\pi}{5}\right.\\ &\left.+2\cos\left(k\frac{\pi}{30}\right)\cos\left(l\frac{\pi}{50} + \frac{\pi}{2}\right)\right]\end{aligned} \tag{38}$$

where $k, l \in \{1, 2, \ldots, 100\}$.

To better show DHODA's performances, we calculate AM and FM estimation errors according to the L^2 norm, the minimum squared error (MSE), and relative variances, between exact components and the estimated ones with the DHODA. As shown in Table 1, demodulation errors with the DHODA are lower than the DESA. Figure 2 shows qualitatively that the amplitude and the horizontal and vertical FM components are well estimated by the DHODA.

Figure 3 shows the application of the DHODA to a noisy and blurred image (Fig. 3a). The histogram is shown in Fig. 3b.

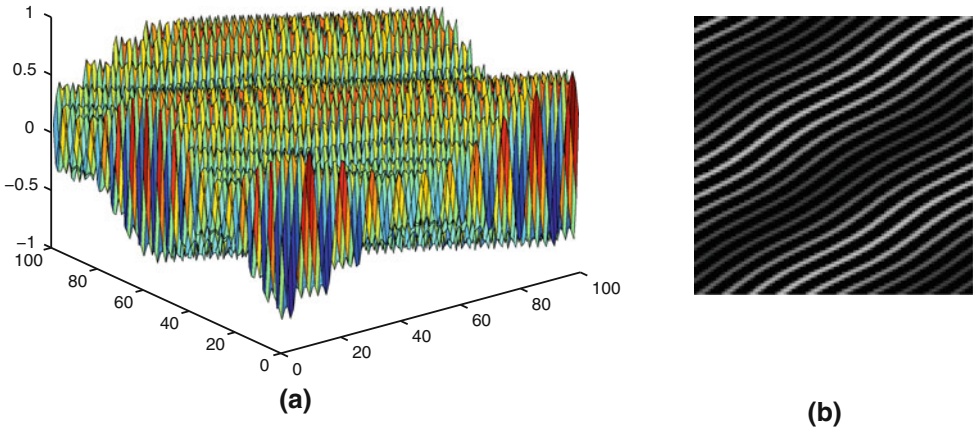

Fig. 1 **a** Perspective plot of original 2D AM–FM signal. **b** Intensity image of the AM–FM signal

Table 1 DHODA and 2D DESA demodulation errors

	$\text{MSE}(a, \hat{a})$	$\|a - \hat{a}\|_2$	$\text{var}\left(\frac{a-\hat{a}}{a}\right)$	$\text{MSE}(\Omega_1, \hat{\Omega}_1)$	$\|\Omega_1 - \hat{\Omega}_1\|_2$
2D DESA	0.0119	119.4173	0.0415	0.0483	482.5965
DHODA	9.9617×10^{-4}	9.9617	0.0044	0.0092	92.1198
	$\text{var}\left(\frac{\Omega_1 - \hat{\Omega}_1}{\Omega_1}\right)$	$\text{MSE}(\Omega_2, \hat{\Omega}_2)$	$\|\Omega_2 - \hat{\Omega}_2\|_2$	$\text{var}\left(\frac{\Omega_2 - \hat{\Omega}_2}{\Omega_2}\right)$	
2D DESA	0.0418	0.0164	164.3891	0.0387	
DHODA	0.0093	0.0059	58.5233	0.0146	

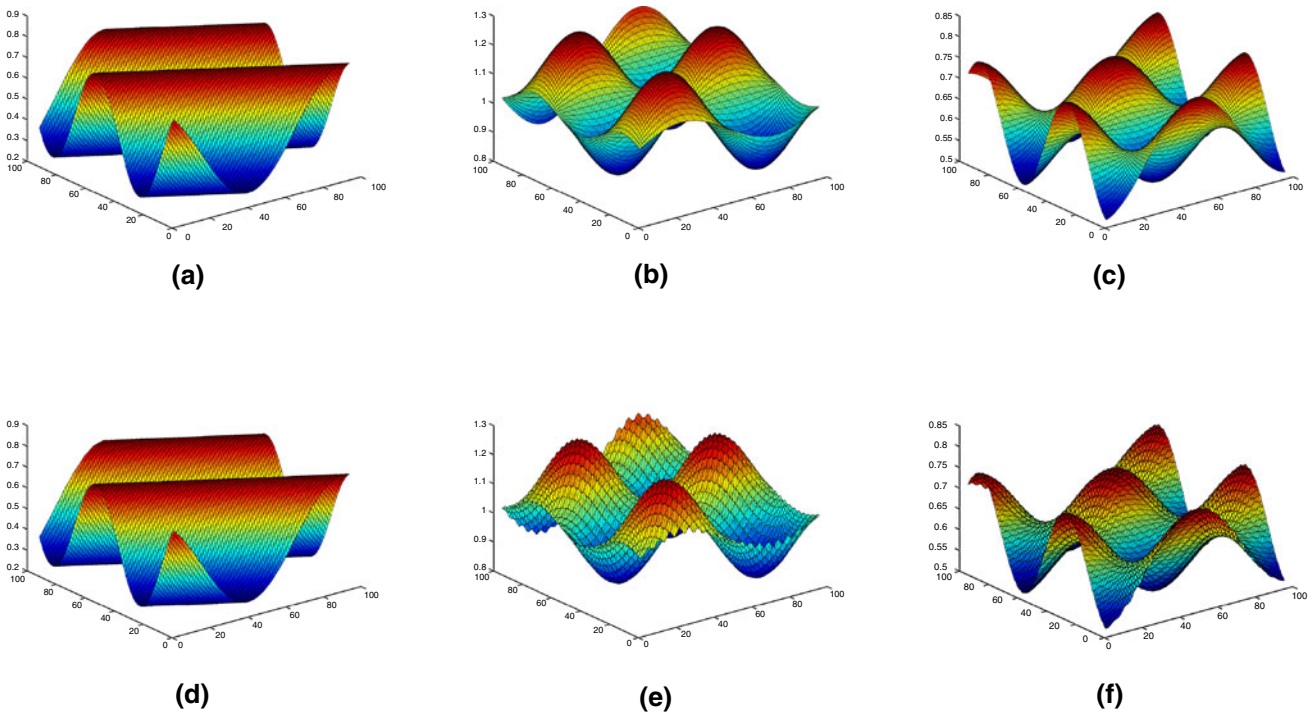

Fig. 2 Plottings of real components versus estimated components. Real components: AM (**a**), Horizontal FM component (**b**), Vertical FM component (**c**). Estimated components with the DHODA: AM (**d**), Horizontal FM component (**e**), Vertical FM (**f**)

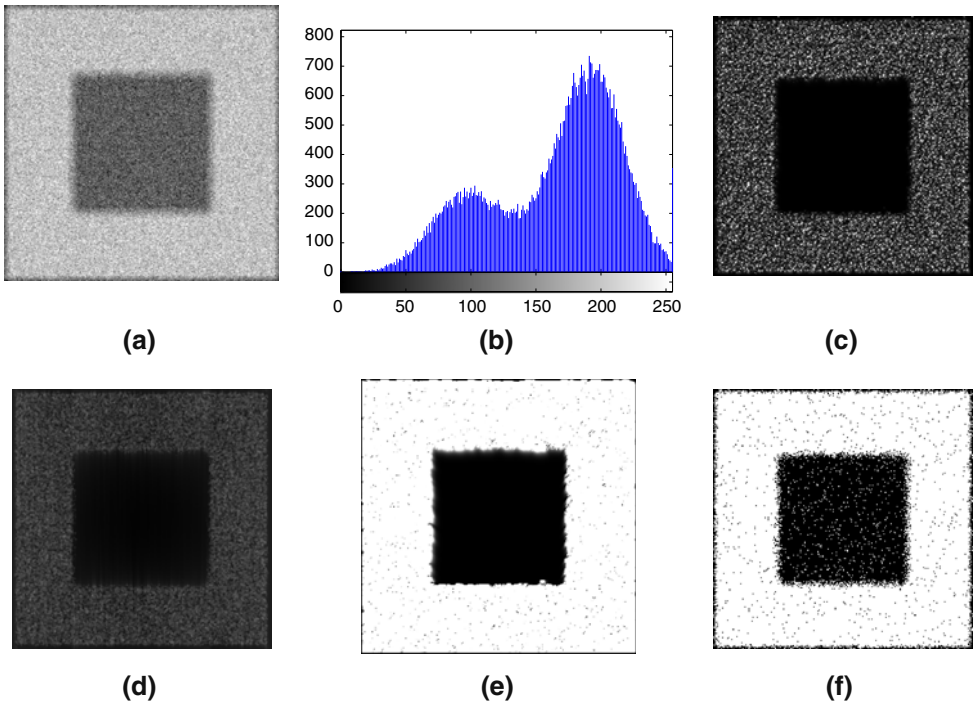

Fig. 3 Black square noisy and blurred image (**a**); Histogram of the image (**b**); AM component obtained with the 2D DESA (**c**); AM component obtained with the AS (**d**); AM component estimated with the DHODA (**e**); Thresholded image (**f**)

We take this image example, because it is simple to analyze and bears some texture. Also, its associated ground truth is known. The AM components of the square image, obtained with the DESA, the AS and the DHODA, are shown in Fig. 3c–e, respectively. For the three demodulation methods, no post-processing of the AM components is performed (Fig. 3c–e). As one notices, the AM component obtained with the DHODA (Fig. 3e) captures the dark square and segments it. Neither the DESA (Fig. 3c) nor the AS method (Fig. 3d) are able to achieve this. We did not expect the AM component to segment any part in the image while using the DESA [5] or the AS [6], but we just put forward the additional and relevant texture information brought out by the 2D DEO in image demodulation, compared to the 2D TKEO and the 2D Hilbert transform.

The segmentation of the dark square could be a difficult task with other segmentation techniques without a preprocessing or a post-processing. To illustrate that fact, we use an image thresholding method for a segmentation issue. Figure 3f shows the thresholding result using the image histogram (cf. Fig. 3b). As one notices, Fig. 3f depicts some noise artifacts on the dark square, the image background, and the image borders. Performing a median filter prior to the thresholding yields a better segmentation, though.

To display the FM counterparts, we use needle diagram plottings, which are much more expressive [6,11]. Diagrams are composed of arrows, and for every pixel, an arrow is drawn at the pixel's neighborhood for clarity. The arrow originates from that pixel, and terminates by an arrowhead. The length of the arrow is inversely proportional to the FM's magnitude (The FM's magnitude is the square root of the sum of the squares of the horizontal and vertical frequency values). With this displaying style, image frequencies make much more sense and are much more conclusive, in comparison to the Fourier transform. For the square image (Fig. 3a), we have, as expected, small arrows of same orientations all around the black square, which mean high-frequency area (Fig. 4). And we have large arrows with also the same orientations inside the black square, which means low frequencies (Fig. 4). This is coherent, because it is an homogeneous zone.

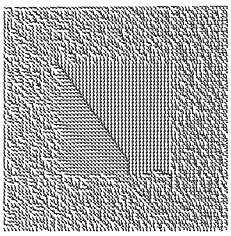

Fig. 4 Needle diagrams depicting FM component of Black square image

4.2 Real images

We show an application of the DHODA to real Sonar images that exhibit non-stationarity in spatially varying contrast and granularity, and also in textured regions. Figure 5a, e, i is an examples of Sonar images showing essentially three regions: echo, mine shadow, and sea-bottom reverberation. In this second part of results, it turns out that the DHODA behaves like a segmentation method. In addition to realistic conditions [5], we add the hypothesis of zero-mean to images. Practically,

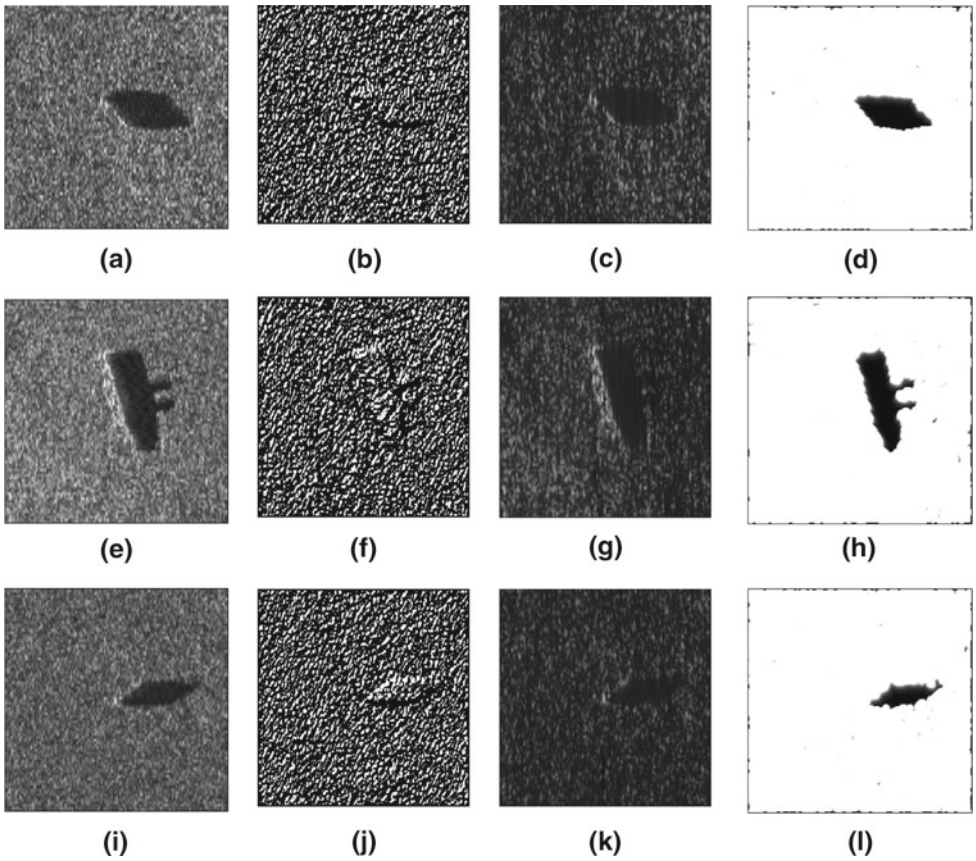

Fig. 5 First Sonar image (**a**), AM components obtained with DESA (**b**), AS (**c**), DHODA (**d**); Second image (**e**), AM components obtained with: DESA (**f**), AS (**g**), DHODA (**h**); Third image (**i**), AM components obtained with: DESA (**j**), AS (**k**), DHODA (**l**)

we subtract from the original image its global mean. As pointed out by Maragos and Bovik, the application of 2D TKEO to narrowband images may yield fewer negative values [5]. Thus, since the DESA requires non-negative energy values for narrowband signals, they [5] suggested to set all negative values to zero. In our numerical simulations, we put each negative value equal to the mean calculated inside a 3×3 window and centered on that negative value. Also, before demodulating real images, we apply a median filter as for a pre-processing. We point out that the same pre-processing is also applied to compared demodulation techniques: the DESA and the AS approach.

As we previously said, the AM component gives information about textures' contrast, that is the intensity disparity between the dark and bright textures, while the FM component captures the local orientation, the image granularity, and edges in the image. For the presented Sonar images, the AM component is conclusive for the segmentation of regions of interests, the mines' shadows. For all the three presented Sonar images, a tiny part of the mine shadow is left over in the segmentation (Fig. 5). To improve the segmentations, a simple window averaging scheme is used as for a post-processing. As shown in Fig. 5, neither the 2D DESA nor the AS method is able to segment the mines' shadow from just the AM component (Fig. 5b, c, f, g, j, k). As we previously said, we did not expect the AM component to segment any part in the image while using the DESA or the AS, but we just would like to reveal the important texture information brought out by the 2D DEO in image demodulation, compared to the 2D TKEO and the 2D Hilbert transform, used, respectively, for the DESA and the AS method. The segmentation results using AM information are illustrated with Fig. 5.

To display FM counterparts obtained with the proposed DHODA, we use again the needle diagram plottings discussed previously. FM plottings of Sonar images (cf. Fig. 5) are shown in Fig. 6. The scale factor of the arrows length is chosen small in order to get more conclusive descriptions of frequencies. Because of the texture characteristics, we have, as expected again, small arrows all around the mines' shadows (Fig. 5b, c, f, g, j, k). This indicates very high frequencies in those regions, which makes sense. On the contrary, we have large arrows in the areas corresponding to the mines' shadows. This implies low frequencies in those areas, which makes also sense, because of the homogeneousness of those regions.

5 Conclusion

In this paper, we have explored the discrete 2D DEO for narrowband image demodulation. A new image demodulation

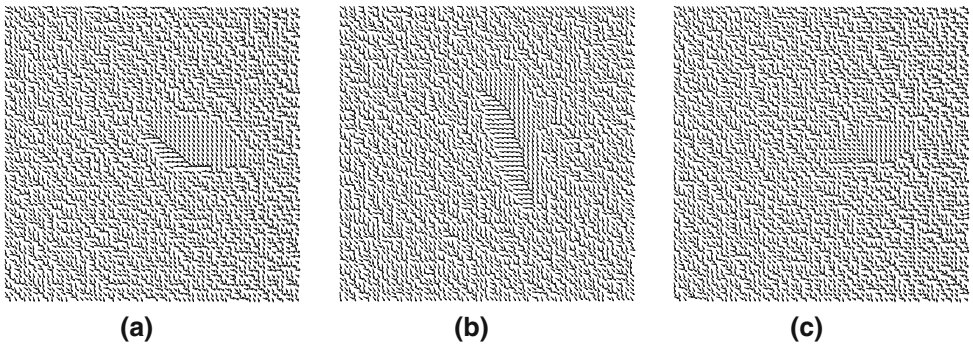

Fig. 6 FM component needle diagram plots of images of Fig. 5a (**a**), e (**b**), and i (**c**)

based on 2D DEO is then presented. As a first result, we show that 2D-DEO brings relevant additional information that cannot be carried out by the classical 2D TKEO and the 2D Hilbert transform, which were used in the DESA and the AS method, respectively. Indeed, as confirmed by the numerical results, the proposed DHODA gives better results for both synthetic and real images than the 2D DESA and the AS approach. Another result regards the proposed demodulation algorithm is the application of the DHODA to image segmentation. In fact, it can be applied in a straightforward way for segmentation of real images; especially, the segmentation of mines' shadows in Sonar images, which is very important for civil and military applications. The segmentation method achieved through the AM component obtained with the DHODA could help for many applications, even though the hole mines' shadows are not fully extracted. We finally show the coherence of frequencies in images. However, like all energy-based demodulation methods, the proposed algorithm is also sensitive in a very noisy environment. So, as future work, we plan to develop a more robust algorithm, based on 2D DEO, that can handle even larger class of wideband images and more robust to noise. We also plan to extend the DHODA to multicomponent images using, for example, a Gabor filtering approach.

Acknowledgments We are grateful to Dr. Joseph P. Havlicek and Dr. Chuong T. Nguyen, from the University of Oklahoma at Norman, for providing the needle diagram codes.

References

1. Teager, H., Teager, S.: Evidence for nonlinear production mechanisms in the vocal tract. In: Speech Production and Speech Modeling, NATO Advanced Study Institute, vol. 55, pp. 241–261. Kluwer, Dordrecht (1990)
2. Kaiser, J.F.: On a simple algorithm to calculate the 'energy' of a signal. In: Proceedings of ICASSP, pp. 381–384 (1990)
3. Yu, T.H., Mitra, S.K., Kaiser, J.F.: A novel nonlinear filter for image enhancement. In: Proceedings of SPIE/SPSE Symposium on Electronic Imaging: Science and Technology, pp. 303–309 (1991)
4. Maragos, P., Kaiser, J.F., Quatieri, T.F.: Energy separation in signal modulations with application to speech analysis. IEEE Trans. Sig. Process. **41**(10), 3024–3051 (1993)
5. Maragos, P., Bovik, A.C.: Image demodulation using multidimensional energy separation. Opt. Soc. Am. A **12**(9), 1867–1876 (1995)
6. Havlicek, J.P.: AM–FM image models. Ph.D. dissertation, The University of Texas at Austin (1996)
7. Maragos, P., Potamianos, A.: Higher order differential energy operators. IEEE Sig. Process. Lett. **2**(8), 152–154 (1995)
8. Salzenstein, F., Montgomery, P., Benatmane, A., Boudraa, A.: 2D discrete high order energy operators for surface profiling using white light interferometry. Proc. ISSPA **1**, 601–604 (2003)
9. Salzenstein, F., Boudraa, A., Cexus, J.: Generalized higher-order nonlinear energy operators. J. Opt. Soc. Am. (A) **24**(12), 3717–3727 (2007)
10. Boudraa, A., Salzenstein, F., Cexus, J.: Two-dimensional continuous higher-order energy operators. Opt. Eng. **44**(11), 7001–7010 (2005)
11. Havlicek, J.P., Tay, P.C., Bovik, A.C.: AM–FM image models: fundamental techniques and emerging trends. In: Bovik, A.C. (ed.) Handbook of Image and Video Processing, chap. 4.4, 2nd edn, pp. 377–395. Elsevier Academic Press, Burlington (2005)
12. Pattichis, M.S., Bovik, A.C.: Analyzing image structure by multidimensional frequency modulation. IEEE Trans. Patt. Anal. Mach. Intell. **29**(5), 753–766 (2007)
13. Kokkinos, I., Evangelopoulos, G., Maragos, P.: Texture analysis and segmentation using modulation features, generative models and weighted curve evolution. IEEE Trans. Patt. Anal. Mach. Intell. **31**(1), 142–157 (2009)
14. Maragos, P., Kaiser, J.F., Quatieri, T.F.: On amplitude and frequency demodulations using energy operators. IEEE Trans. Sig. Process. **41**(4), 1532–1550 (1993)